Distribution of Morphology and Transport Properties of Water Vapor in Injection-Molded Biodegradable Aliphatic Polyester

Maria Partini, Giuliana Gorrasi, Roberto Pantani

Department of Chemical and Food Engineering, University of Salerno, Via Ponte don Melillo, Fisciano (SA) 84084, Italy

Received 7 November 2009; accepted 22 January 2010
DOI 10.1002/app.32137
Published online 27 April 2010 in Wiley InterScience (www.interscience.wiley.com).

ABSTRACT: A biodegradable polyester, poly(tetramethylene dodecanedioate), was injection molded in a rectangular cavity. Thin sections were sliced from molded samples starting from the skin. The morphology distribution inside the molded samples was studied by X-ray analysis. The diffusion and solubility coefficient of water vapor were then measured using the microgravimetric method at the temperature of 30°C. Results show that morphology developed during the process influences the diffusion of water molecules through the polymer matrix. In particular, a direct influence of crystalline degree on the sorption and diffusion parameters was identified. © 2010 Wiley Periodicals, Inc. J Appl Polym Sci 117: 2831–2838, 2010

Key words: biodegradable; diffusion; injection molding; polyesters; morphology

INTRODUCTION

Biodegradable polymers have attracted increasing interest in fundamental research as well as in technology, due to their potential in addressing environmental concerns and biomedical applications. Biodegradable polymers break down in physiological environments by macromolecular chain scission into smaller fragments, and ultimately into simple, stable end-products. The degradation may be due to aerobic or anaerobic microorganisms, biologically active processes (e.g., enzyme reactions) or passive hydrolytic cleavage. The last two decades of polymer technology have seen a sharp rise in the development and commercial marketing of such new materials.[1,2] Aliphatic polyesters are amongst the most important biocompatible and biodegradable materials that have received increasing attention. Their applications in conventional fields, such as agriculture, packaging, and fiber, and biomedical fields, e.g., tissue engineering, surgical suture, gene therapy, and controlled drug delivery, have grown significantly due to the availability of novel products with better performance characteristics.[1–6] Almost all biodegradable polyesters are semicrystalline, and therefore, crystallization is a key process affecting their physical properties. The crystallization behavior of biodegradable polyesters has been extensively investigated in recent decades. Generally, the physical properties of thermoplastic polymers such as thermal, mechanical properties, and biodegradability (of biodegradable polymers) are considerably influenced by the crystalline structure and morphology that can be manipulated by changing the crystallization conditions. Accordingly, studies on the relationships between structure, morphology, and properties are of fundamental importance for controlling the final properties of polymeric materials. The study of the influence of crystallinity and orientation on the transport properties of gases and vapors in polymeric films is very important both theoretically and technologically.[7–10] Sorption and diffusion determine the permeability of a film, and this parameter is of fundamental importance if the film has to be used as packaging material. The food packaging industry needs particular performances of the materials selected, particularly in terms of the barrier requirements.[11–16] Both crystallinity and molecular orientation generally decrease the permeability, due to decreased sorption and/or diffusion. In most cases the crystalline regions were found impermeable to the vapor penetrants.[7–10] The aim of this work was to use the injection molding technology to process a biodegradable polyester: Poly(tetramethylene dodecanedioate). The distribution of morphology (in terms of degree of crystallinity and orientation) was investigated on thin slices cut from molded samples from the skin part of the molded slab along the flow direction. To detect the amount and distribution of

Correspondence to: M. Partini (mpartini@unisa.it).

TABLE I
Properties of the Polyester Adopted in This Work

M_n (g/mol)	M_w (g/mol)	M_z (g/mol)	M_w/M_n	M_z/M_w	T_m[a] (°C)	T_c[a] (°C)	T_g[b] (°C)
20,000	45,000	90,000	2.3	2.0	66	47	−23

[a] Peak value of a DSC thermogram at 10°C/min.
[b] From a DSC thermogram at 10°C/min.

the amorphous permeable phase, transport properties (sorption and diffusion) of water vapor were investigated using microgravimetric method at the temperature of 30°C.

EXPERIMENTAL

Material

The polymer analyzed in this work is a Poly(tetramethylene dodecanedioate)

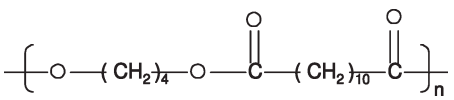

(1)

Table I shows the main physical properties.

The degradation in the molten and the hydrolytic degradation in the solid state of this material were studied in previous works.[17,18]

Processing

Film specimens (0.090–0.050 mm thick) were prepared by compression molding at 120°C under a pressure of 10 bar.

The injection molding of the samples was carried out on a HAAKE MiniJet Molding Machine. A rectangular mold was used to produce a slab having the following dimensions: length, 75 mm; width, 12.5 mm; thickness, 1 mm. The injection molding experiments were carried out by keeping the melt temperature at 120°C, the mold temperature at 30°C, the injection and holding pressures at 140 bar. The mold and injection temperatures were chosen to allow a complete cavity filling under the applied injection pressure. A previous rheological characterization of the material allowed to exclude any possible material degradation under the chosen thermal conditions.[19] The cavity filling lasted about 1 s. At the end of the filling stage, a holding pressure was applied to compensate for the shrinkage due to cooling and crystallization. The holding time was always 10 s. Normally, since solidification proceeds from the surface to the core of the sample, the filling stage induces a higher orientation in the layers close to the surface, but the holding pressure can also induce an orientation in the layers close to the midplane.[20] An unoriented sample, taken as reference, was obtained by hot pressing in a Carver laboratory press the material's pellets at 120°C at pressure of 10 bar, followed by cooling at a rate of about 1°C/s to room temperature.

The microstructure of the obtained samples is shown in Figure 1, where a micrograph of a slice cut in a position close to the injection point, is reported. The micrograph refers to half thickness of the sample, the flow direction being vertical. The picture shows the typical skin-core structure of molded samples with an oriented region (the brightest band close to the surface) and a much less oriented core. The samples were microtomed into 100-μm thick slices, starting from the surface and successively getting deeper until the last slice was in the center according to the scheme of Figure 2.

The first slice obtained, corresponding to the skin layer was coded as Section 1, the second slice was coded as Section 2, the forth slice, corresponding to the core of the sample, was coded as Section 4.

All the samples were dried under vacuum at 30°C for 48 h before any measurement.

Methods of investigation

Crystallinity and crystalline orientation of the slices cut from injection-molded samples and of the compression-molded films were analyzed by WAXD. X-ray diffraction analysis was performed by using

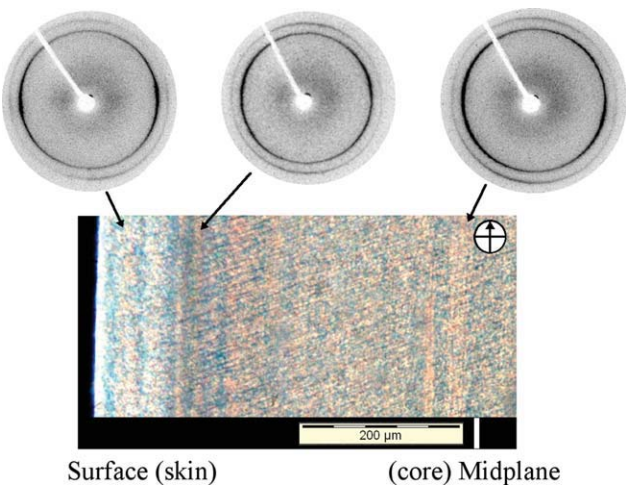

Figure 1 Optical micrograph under polarized light of half of the cross section of the molded sample. The 2D WAXD patterns refer to the positions indicated by the arrows. [Color figure can be viewed in the online issue, which is available at www.interscience.wiley.com.]

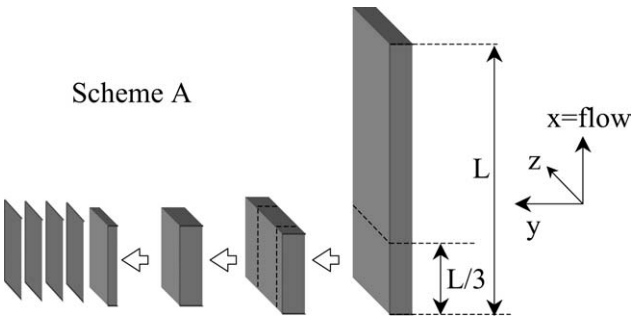

Figure 2 Sample preparation from injection molding specimens.

XRD (RINT, Rigaku, Japan) using Cu Kα radiation (40 keV, 20 mA). The exposure time was 1 h.

Two-dimensional WAXD patterns were circularly averaged to generate plots of diffracted intensity as a function of angle 2θ. The polymer presents a polyethylene-like crystal structure: the Bragg angle of (110) reflection corresponds to $2\theta = 21.2$, the Bragg angle of (200) corresponds to $2\theta = 24.3$, the Bragg angle of (020) corresponds to $2\theta = 35.2$. By calculating the d spacing for each reflection from Bragg's law and by applying the relation between the d spacing and unity cell parameters for an orthorhombic system, it was possible to evaluate the unit cell parameters as $a = 7.33$ Å and $b = 5.11$ Å.

When considering injection-molded samples, the c-axis (chain) orientation in the direction of flow (machine direction, MD) must be considered. Without the pure reflections from the c-axis, Wilchinsky's[21] method was used to obtain information about the c-axis orientation:

$$\langle \cos^2 \phi_{c,Z} \rangle = 1 - 0.514 \langle \cos^2 \phi_{200} \rangle - 1.486 \langle \cos^2 \phi_{110} \rangle \quad (2)$$

where $\langle \cos^2 \phi_{c,Z} \rangle$ was calculated from the strong (110) and (200) reflections, using the angle between the normal of the (110) plane and the a-axis and the orthogonality relationship in the orthorhombic crystal structure:

$$\langle \cos^2 \phi_{a,Z} \rangle + \langle \cos^2 \phi_{b,Z} \rangle + \langle \cos^2 \phi_{c,Z} \rangle = 0 \quad (3)$$

To identify a preferred orientation of crystallites, WAXD photographs on selected samples were analyzed. Azimuthal scans of Bragg reflections were obtained. The orientation was obtained in terms of Hermann's factor f:

$$f_\phi = \frac{3\langle \cos^2 \phi_{c,Z} \rangle - 1}{2} \quad (4)$$

where ϕ is the angle between the unit within a crystal of interest (e.g., chain axis c) and a reference axis (e.g., fiber or machine direction). $\cos^2\phi$ is defined as follows:

$$\langle \cos^2 \phi_{c,Z} \rangle = \frac{\int_0^{90^\circ} \left(I(\phi) sen\phi \cos^2 \phi\right) d\phi}{\int_0^{90^\circ} \left(I(\phi) sen\phi\right) d\phi} \quad (5)$$

When chains are perfectly aligned along the reference axis $f = 1$, whereas $f = -1/2$ for chains aligned perpendicular to the reference axis. For random orientation, $f = 0$.

Transport properties experiments were performed using a conventional McBain spring balance system, which consists of a glass water-jacketed chamber serviced by a high vacuum line for sample degassing and penetrant removal.[22] Inside the chamber, the samples were suspended by a helical quartz spring supplied by Ruska Industries, Inc. (Houston, TX) with a spring constant of 1.892 cm/mg. The temperature was controlled to 30 ± 0.1°C by a constant temperature water bath. Before beginning the sorption experiments, the sample was exposed to vacuum for at least 24 h to remove previously sorbed air gasses and water vapor from the polymer. Liquid penetrant was subjected to several freeze-thaw cycles to remove dissolved gases. Then, the sample was exposed to the penetrant at fixed pressures, and the spring position was recorded as a function of time using a cathetometer. The spring position data were converted to mass uptake data using the spring constant. Diffusion coefficients and equilibrium mass uptake were extracted from these kinetic sorption data. Sorption experiments were performed on 100-μm thick slices cut according to the scheme presented in Figure 2. Experiments were also performed on compression-molded films. All the data presented were averaged on at least three samples.

RESULTS AND DISCUSSION

Structural organization

The X-ray diffractogram of the compression-molded sample of the polymer is reported in Figure 3. The diffractogram was analyzed by a deconvolution procedure performed according to a scheme reported in the literature.[23] The full spectrum was considered as a superposition of the number of reflections due to each phase present (three reflections were considered, two for the crystalline phase corresponding to $2\theta = 21.17, 24.28$, one for the amorphous halo) each reflection being described by a combination of a Lorentzian function and a Gaussian function. The positions of all the peaks and their shapes (namely the percentage of Gaussian function) were kept constant

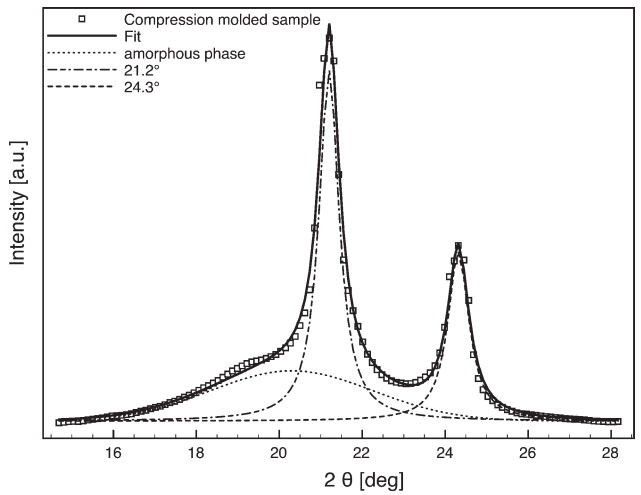

Figure 3 X-ray diffrattogram of a poly(tetramethylene dodecanedioate) compression-molded film sample. The results of the deconvolution are also shown.

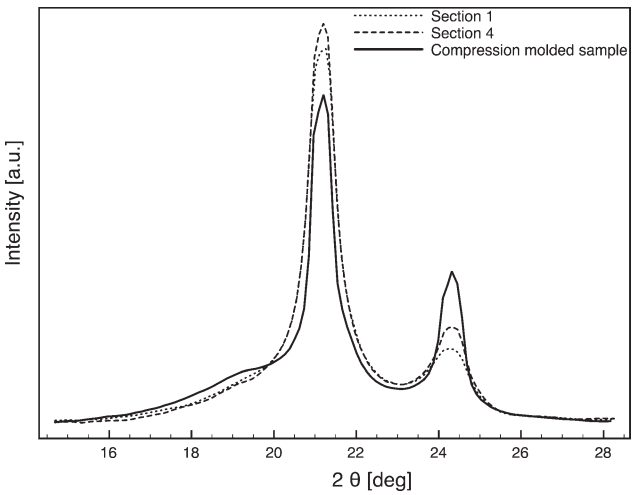

Figure 4 The deconvolution patterns for compression-molded film sample and of films sliced from an injection-molded sample.

for all the samples. The crystallinity degree was calculated as the sum of the areas of the crystalline peaks divided by the total area below the spectrum.

The parameters defining each reflection were determined, with a general purpose optimization routine, adopting as objective function the total quadratic error with respect to the experimental spectrum. Deconvolution results are affected by some uncertainty which was estimated as ±3% on the percentage crystalline phase. The crystallinity of the compression-molded sample resulted to be 66%.

The circular averages of the 2D WAXD for Sections 1 and 4 are shown in Figure 4 together with the spectrum of the compression-molded sample. The two slices of the molded sample presented very similar spectra, even if the peaks of the Section 1 are less pronounced, thus revealing a lower crystalline content, which can be attributed to the much higher cooling rate experienced by the skin layers with respect to the core sections. If compared with the compression-molded sample, the sections of the molded sample present peaks width significantly larger, especially those corresponding to the (200) reflection ($2\theta = 24.3°$). This clearly indicates smaller crystal size and/or lower crystal perfection. This observation is consistent with a much larger nucleation rate induced by flow during injection molding and with a higher cooling rate experienced by the sample inside the mold. Furthermore, the pattern of the section 1 (skin region) presented clear intensity variations along the azimuthal angle, thus revealing a significant orientation. These intensity variations become weaker going from the skin to the core region of the sample.

The results of the analysis of crystalline distribution and orientation along the thickness of injection-molded samples are reported in Table II. Crystallinity resulted to be quite uniformly distributed along the thickness of the samples. The crystallinity degree inside the molded sample resulted to be much higher with respect to the compression molded one. This can be ascribed to the nucleating effect of flow, or possibly to the enhancement effect of pressure on crystallization kinetics.

Orientation is present in all the thickness of the specimens, even if it is slightly decreasing going from the skin to the core, as expected. The analysis of orientation for compression-molded sample provided a $f_c = 0.07$, confirming the absence of a preferential orientation of these samples.

Transport properties

The transport properties were measured at three different relative humidity: RH as $P/P^{sat} = 0.2, 0.4, 0.6$, where P is the pressure in the apparatus and P^{sat} is the vapor pressure of water at 30°C.

The water diffusion coefficient was evaluated for $M_t/M_\infty < 0.6$, by the equation:

$$\frac{M_t}{M_\infty} = 4\left(\frac{Dt}{\pi l^2}\right)^{1/2} = \left(\frac{16D}{\pi l^2}\right)^{1/2} t^{1/2} \qquad (6)$$

TABLE II
Crystallinity and Crystal Orientation of Compression-Molded Sample and of the Sections of Injection-Molded Sample

Sample	f_c	X_c
Compression-molded film	0.07	0.66
Section 1	0.32	0.82
Section 2	0.22	0.84
Section 4	0.20	0.85

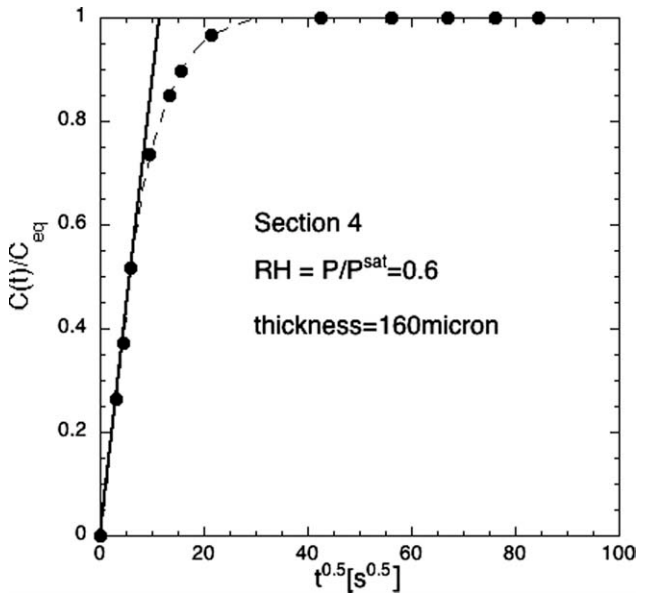

Figure 5 Sorption kinetic curve ($C(t)/C_{eq}$ vs. the square root of time) for the Section 4 of the molded sample at relative humidity, RH, of 0.60%.

where M_t and M_∞ are weight variations at time t and at equilibrium, respectively, l is the sample thickness and D the diffusion coefficient.

Figure 5 reports the sorption kinetic curve ($C(t)/C_{eq}$ vs. the square root of time) for the Section 4 of the molded sample at relative humidity, RH, of 0.60, as representative of all the samples. All the samples showed a Fickian behavior during the sorption of water vapor at different activities, so it was possible to derive, for each activity, a diffusion coefficient D(C) following the eq. (6). For the polymer-solvent system, the diffusion parameter is usually not constant but depends on the solvent sorbed concentration, according to the empirical equation:

$$D = D_0 \exp(\gamma C_{eq}) \tag{7}$$

where D_0 is the zero concentration diffusion coefficient (related to the fractional free volume and to microstructure of the polymer), γ is a coefficient which depends on the fractional free volume and on the effectiveness of penetrant to plasticize the matrix, and C_{eq}(g/100 g) the water vapor equilibrium concentration.

The equilibrium concentration of water vapor as a function of the relative humidity is reported in Figure 6.

The sorption curves of compression-molded films follow a Langmuir-mode sorption behavior: at low activity (up to RH = 20%) an increase of water concentration indicates that besides the normal dissolution process, the solvent also occurs on preferential sites in which the molecules are adsorbed and/or immobilized. It is assumed that these specific sites on the matrix have a finite capacity. The sections of injection-molded samples showed a Flory-Huggins behavior. In this case the interactions between the diffusing molecules are stronger than the penetrant-polymer interaction and the solubility coefficient increases continuously with pressure. It is of interest to observe that the value of equilibrium concentration for the first slices is always higher than that of slices from inner position.

Figure 7 reports the diffusion parameter, D [m^2/s], as a function of the concentration of sorbed water, C_{eq} (g/100 g), for all the samples. Calculated values show a general increase of the diffusion coefficients on increasing C_{eq} (g/100 g).

According to eq. (7), D_0 was obtained by extrapolation to zero vapor concentration. Figure 8 reports the extrapolated diffusion parameters vs. the crystallinity. The diffusion parameter decreases as the crystallinity increases. The effect of orientation cannot be easily evinced from data analysis and is surely subordinate to the effect of X_c.

The relationship between the coefficient γ and the crystalline degree is reported in Figure 9. The parameter γ increases with the crystalline degree: the fractional free volume and the effectiveness of penetrant to plasticize the matrix are indeed related to crystalline degree of the polymer. Such trend is very interesting and unexpected. We can hypothesize that the crystalline domains tend to aggregate and to separate from the amorphous phase with increasing the crystallinity degree; as consequence the amorphous domains show a more pronounced swelling behavior with respect to the solvent.

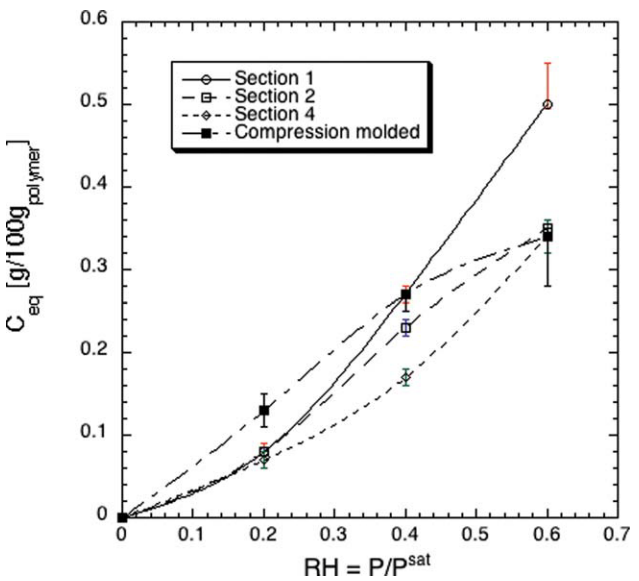

Figure 6 Sorption isotherm of water vapor at $T = 30°C$. [Color figure can be viewed in the online issue, which is available at www.interscience.wiley.com.]

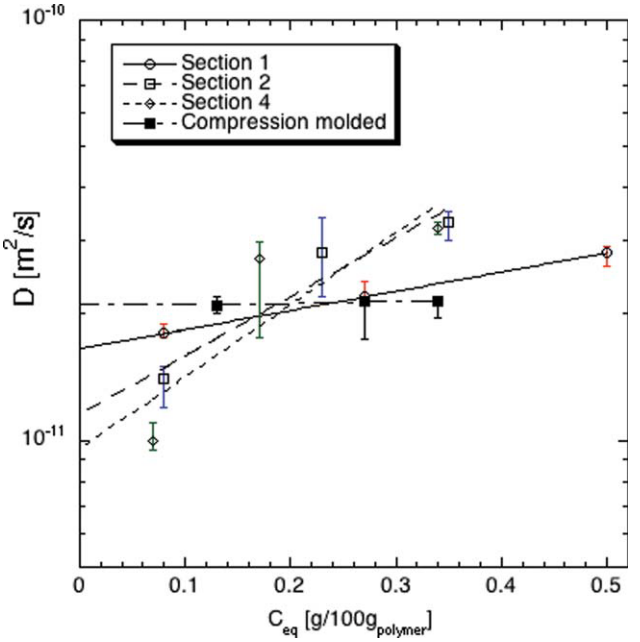

Figure 7 Diffusion coefficient as function of concentration of sorbed water (C_{eq}). [Color figure can be viewed in the online issue, which is available at www.interscience.wiley.com.]

Figure 10 reports the solubility at low relative humidity (RH = 20%) versus the cristallinity. As expected, there is a direct influence of crystallinity on the sorption parameter: the variations of the amorphous phase density, and therefore of the fractional free volume estimated for the amorphous phase are related to the crystallinity of the samples. The solubility linearly decreases as the crystallinity increases, namely the fraction of phase that is permeable to water vapor decreases with crystallinity. Furthermore, the extrapolated value of C_{eq} at $X_c = 1$ is nearly zero. This result is consistent with the relationship:

$$C_{eq} = C^*_{eq} X_a \tag{8}$$

where C^*_{eq} is the coefficient of solubility in a completely amorphous polymer and X_a is the fraction of

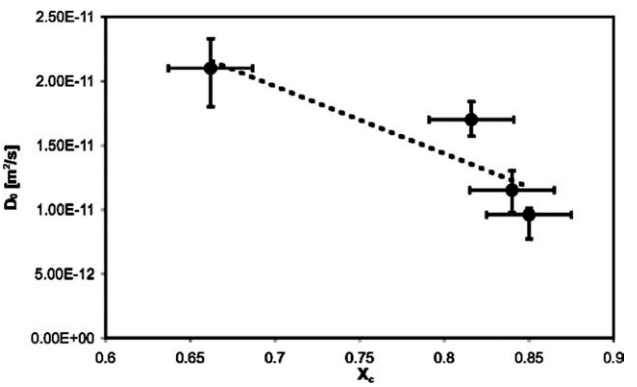

Figure 8 Extrapolated diffusion parameters (D_0) as function of X_c.

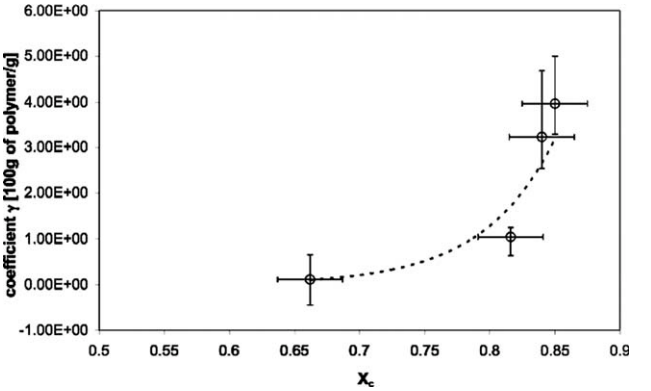

Figure 9 Relationship between coefficient γ and crystalline degree.

the amorphous phase of the polymer. Because it was not possible to obtain experimentally a fully amorphous sample, we estimated C^*_{eq} from molar water content of polymer structural unit, as reported by van Krevelen[24] and Piringer.[25] The estimation was performed by taking into account the water sorption capacity of the CH_2 and COO— groups of the polymer repeat unit and the total COOH end group content of the polymer.

Molar water contents of structure group reported by Piringer,[25] at the relative humidity of 20%, were used. In such a manner, the molar water content of a repeat unit of poly(tetramethylene dodecanedioate) was estimated as follows:

$$n_{CH_2} \cdot m_{CH_2} + 2m_{COO-} = m_{H_2O} \tag{9}$$

where:

n_{CH_2} is the number of CH_2 groups in the polymer chain

m_{CH_2} is the molar water sorption capacity of CH_2 groups

m_{COO-} is the molar water sorption capacity of COO—

m_{H_2O} is the molar water content of the polymer per repeat unit of polymer

The water content of polymer, reported in (g of water/100 g of polymer) was the calculated by taking into account the contribution of [COOH] end groups to water sorption:

$$(m_{H_2O}/(PM_u) + x_{COOH} \cdot m_{COOH}) PM_{H_2O} \times 100 = C^*_{eq} \tag{10}$$

where:

PM_u is the molecular weight of the repeat unit

m_{COOH} is the molar water sorption capacity of COOH

x_{COOH} represents the moles of carboxylic terminal groups per grams of polymer

PM_{H_2O} is the molecular weight of water

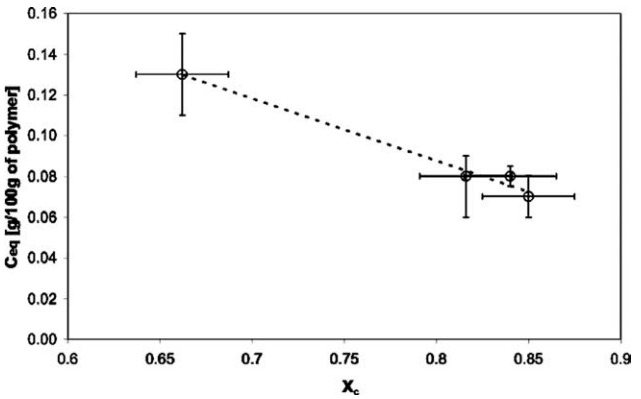

Figure 10 Values of solubility at low C_{eq} relative humidity (RH = 20%) as function of X_c.

The value of C^*_{eq} so estimated was 0.17 g of water/100 g of polymer, which is about 1.5 times the result obtained by extrapolating the linear fitting of Figure 10 to zero crystallinity level. This would mean that all the amorphous phase is permeable to water.

Apart from the effect on solubility, the dispersed crystalline phase presents a resistance to the permeant passage. More exactly, these crystalline zones have two effects on the gasses diffusion. On one hand, they increase the effective path length of diffusion, and, on the other hand, they seem to reduce the polymer chains mobility in the amorphous phase (because chain ends are trapped in the neighboring crystalline lamellae) and, then, lead to a higher activation energy of diffusion. To account for these effects, Michaels and coworker[26] introduced a "tortuosity factor" τ and a "chain immobilization factor" β. They proposed the following expressions for the coefficients of solubility and diffusion:

$$D = D^*/(\beta\tau) \tag{11}$$

where D^* is the coefficient of diffusion in a completely amorphous polymer.

We estimated D^* at 30°C from the molar activation energy of diffusion, E_D, the molecular diameter σ_{H2O} of water vapor and the glass transition T_g of the polymer as reported by van Krevelen[24]:

$$10^{-3}\frac{E_D}{R} = \left(\frac{\sigma_{H_2O}}{\sigma_{N_2}}\right)^2 \left[7.5 - 2.5 \times 10^{-4}\left(T_g - 298\right)^{3/2}\right] \pm 1.0 \tag{12}$$

$$\log D^* = 10^{-3}\frac{E_D}{R} - 5 \pm 0.8 \tag{13}$$

$$\log D(T) = \log D^* - \frac{435}{T} \cdot 10^{-3}\frac{E_D}{R} \tag{14}$$

where E_D molar is the activation energy of diffusion, σ_{H_2O} and σ_{N_2} the molecular diameter of water vapor and nitrogen, T_g the glass transition temperature Poly(tetramethylene dodecanedioate), R the constant of ideal gas. The value of D^* so obtained was 3.5 10^{-10} m^2/s.

From eq. (11), the product of "tortuosity factor" τ and "chain immobilization factor" β was calculated. Figure 11 reports $\tau \cdot \beta$ as function of X_c.

The product of "tortuosity factor" τ and "chain immobilization factor" β, increases with crystalline degree. This is a clue that the more tortuous pathway that a diffusing molecule must take in a semicrystalline polymer increases with the crystallinity.

Results of sorption previously estimated do not show a clear relation with the crystalline orientation in terms of Hermann's factor.

CONCLUSIONS

Transport properties, sorption and diffusion of water vapor, for a biodegradable aliphatic polyester were analyzed. The polymer was injection molded in a simple rectangular cavity. Thin films (slices) were cut from molded samples from the skin part of the molded slab along flow direction. As a reference, also non oriented films were obtained by compression molding. The resulting morphology of the samples was carefully characterized by WAXD analysis. A distribution of morphology was detected inside the molded sample. In particular, the crystalline orientation degree was found to decrease on going from the skin to the core of the sample, whereas a slight increase of crystallinity was found in the same direction. The diffusion and solubility coefficient of water vapor were then measured using the microgravimetric method at the temperature of 30°C. The results show that the distribution of morphology inside the sample determine a distribution of transport. In particular, the crystallinity degree is the main factor affecting all the main aspects of the sorption kinetics. No relevant effect of the crystalline orientation could be detected by data analysis.

NOMENCLATURE

C_{eq}	water concentration in the solid, g/g of polymer
C^*_{eq}	water concentration completely amorphous polymer, g/g of polymer
d	distance between planes, nm
D	coefficient of diffusion, $m^2\ s^{-1}$
D_0	zero concentration diffusion, $m^2\ s^{-1}$
D_a	coefficient of diffusion in a completely amorphous polymer, $m^2\ s^{-1}$
D^*	pre exponential term of the Arrhenius equation for temperature dependence of D, $m^2\ s^{-1}$
E_D	activation energy of diffusion, J/mol

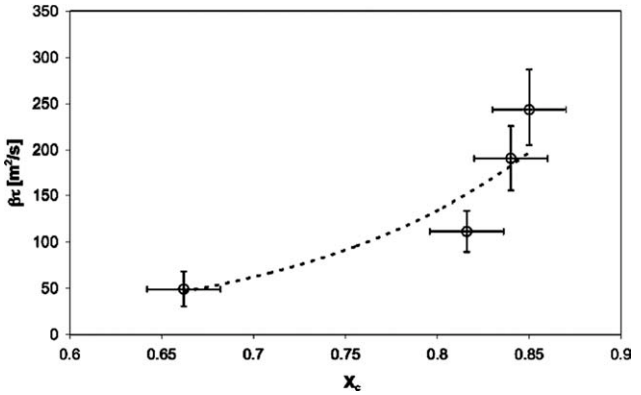

Figure 11 $\tau \cdot \beta$ as function of crystalline degree X_c.

f Hermann's factor
l thickness of the sample, m
m mass, g
m_{CH_2} molar water sorption capacity of CH_2 groups, mol/repeat unit of polymer
m_{COO-} molar water sorption capacity of COO—, mol/repeat unit of polymer
m_{COOH} molar water sorption capacity of COOH, mol/unit
m_{H_2O} molar water content of the polymer per repeat unit of polymer, mol/ repeat unit of polymer
M_0 initial mass of the sample, g
M_∞ amount of water sorbet at equilibrium, g
M_n number average molecular weight, g/mol
M_t amount of water sorber at time t, g
M_w weight average molecular weight, g/mol
M_z average molecular weight, g/mol
N normality of solution, mol/m^3
n_{CH_2} number of CH_2 groups in the polymer chain
P vapor pressure, Pa
P_{sat} vapor pressure of water at 30°C, Pa
PM_{H_2O} molecular weight of water
PM_u weight of repeat unit, g/repeat unit of polymer
R gas universal constant, J/mol^{-1} K^{-1}
t time, s
T temperature, K
T_c crystallization temperature, K
T_g glass transition temperature, K
T_m melting temperature, K
x_{COOH} moles of carboxylic terminal groups per grams of polymer
X_a fraction of the amorphous phase of the polymer
X_c overall crystalline degree

Greeks

β "chain immobilization factor" as defined in eq. (11)
γ coefficient introduced in eq. (7)
θ diffraction semi-angle
λ wavelength of radiation, nm
σ_{H_2O} molecular diameter of water vapor, nm
σ_{N_2} molecular diameter of nitrogen, nm
τ "tortuosity factor" as defined in eq. (11)
ϕ azimuthal angle

References

1. Nair, L. S.; Laurencin, C. T. Prog Polym Sci 2007, 32, 762.
2. Doi, Y.; Steinbüchel, A. Biopolymers, Vol 4, Polyesters III-Applications and Commercial Products; Wiley-VCH: Weinheim, Germany, 2002.
3. Im, S. S.; Kim, Y. H.; Yoon, J. S.; Chin, I. J. Bio-Based Polymers: Recent Progress; Wiley-VCH: New York, 2005.
4. Ikada, Y.; Tsuji, H. Macromol Rapid Commun 2000, 21, 117.
5. Misra, S. K.; Valappil, S. P.; Roy, I.; Boccaccini, A. R. Biomacromolecules 2006, 7, 2249.
6. Iwata, T.; Doi, Y. Macromol Chem Phys 1999, 200, 2429.
7. Crank, J.; Park, J. S. Diffusion in Polymers; Academic Press: London, 1968.
8. Peterlin, A. J Macromol Sci Phys 1975, 1, 57.
9. Rogres, C. E. In Polymer Permeability; Comyn, J., Ed.; Elsevier: Belfast, 1985; Chapter 2.
10. Hopfenberg, H. B. Permeability of Plastic Films to Gases Vapors and Liquids; Plenum Press: New York, 1974.
11. Salame, M. Polym Eng Sci 1986, 26, 1543.
12. Stannett, V. T. Polym Eng Sci 1978, 18, 1129.
13. Lee, W. M. Polym Eng Sci 1980, 20, 65.
14. Lee, S. Y.; Kim, S. C. Polym Eng Sci 1997, 37, 463.
15. Weinkauf, D. H.; Paul, D. R. Macromolecules 1992, 30, 837.
16. Weinkauf, D. H.; Kim, H. D.; Paul, D. R. Macromolecules 1992, 25, 788.
17. Partini, M.; Pantani, R. Polym Degrad Stab 2007, 92, 1491.
18. Partini, M.; Pantani, R. Polym Bull 2007, 59, 403.
19. Partini, M.; Argenio, O.; Coccorullo, I.; Pantani, R. J Therm Anal Calorim 2009, 98, 645.
20. Pantani, R.; Speranza, V.; Sorrentino, A.; Titomanlio, G. Macromol Symp 2002, 185, 293.
21. Alexander, L. E. X-ray Diffraction Methods in Polymer Science; Wiley Interscience: New York, 1969.
22. Felder, R. M.; Huvard, G. S. Permeation, diffusion, and sorption of gases and vapors. In Methods of Experimental Physics: Polymers; Fava, R. A. Ed.; Academic Press: New York, 1980, p 315.
23. Murty, N. S.; Minor, H. Polymer 1990, 31, 996.
24. Van, K. Properties of Polymers, 3rd ed.; Elsevier Science Publishing: London, 1990.
25. Piringer, O.; Baner, A. L. Plastic Packaging Materials for Food; Wiley-VCH: Weinheim, Germany, 2000; p 260.
26. Michaels, A. S.; Parker, R. B., Jr. J Polym Sci 2003, 41, 53.